ACS Catalysis

Research Article

pubs.acs.org/acscatalysis

Kinetics and Mechanism of Alcohol Dehydration on γ-Al_2O_3: Effects of Carbon Chain Length and Substitution

Minje Kang, Joseph F. DeWilde, and Aditya Bhan*

Department of Chemical Engineering and Materials Science, University of Minnesota—Twin Cities, 421 Washington Avenue SE, Minneapolis, Minnesota 55455, United States

Supporting Information

ABSTRACT: Steady-state rates of ether formation from alcohols (1-propanol, 2-propanol, and isobutanol) on γ-Al_2O_3 at 488 K increase at low alcohol pressure (0.1−4.2 kPa) but asymptotically converge to different values, inversely proportional to water pressure, at high alcohol pressure (4.2−7.2 kPa). This observed inhibition of etherification rates for C_2−C_4 alcohols on γ-Al_2O_3 by water is mechanistically explained by the inhibiting effect of surface trimers composed of two alcohol molecules and one water molecule. Unimolecular dehydration of C_3−C_4 alcohols follows the same mechanism as that for ethanol and involves inhibition by dimers. Deuterated alcohols show a primary kinetic isotope effect for unimolecular dehydration, implicating cleavage of a C−H bond (such as the C_β−H bond) in the rate-determining step for olefin formation on γ-Al_2O_3. Bimolecular dehydration does not show a kinetic isotope effect with deuterated alcohols, implying that C−O or Al−O bond cleavage is the rate-determining step for ether formation. The amount of adsorbed pyridine estimated by in situ titration to completely inhibit ether formation on γ-Al_2O_3 shows that the number of sites available for bimolecular dehydration reactions is the same for different alcohols, irrespective of the carbon chain length and substitution. 2-Propanol has the highest rate constant for unimolecular dehydration among studied alcohols, demonstrating that stability of the carbocation-like transition state is the primary factor in determining rates of unimolecular dehydration which concomitantly results in high selectivity to the olefin. 1-Propanol and isobutanol have olefin formation rate constants higher than that of ethanol, indicating that olefin formation is also affected by carbon chain length. Isobutanol has the lowest rate constant for bimolecular dehydration because of steric factors. These results implicate the formation and importance of di- and trimeric species in low-temperature dehydration reactions of alcohols and demonstrate the critical role of substitution and carbon chain length in determining selectivity in parallel unimolecular and bimolecular dehydration reactions.

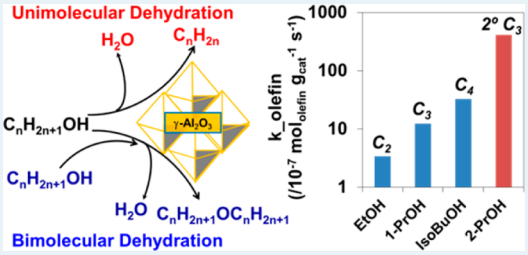

KEYWORDS: *alcohol dehydration, γ-alumina, kinetics and mechanism, multimer inhibition, transition state, carbocation stability, site requirements*

1. INTRODUCTION

Gamma-alumina (γ-Al_2O_3) is a widely used heterogeneous catalyst and catalyst support because of its thermal stability and high surface area.[1−4] Infrared (IR) and nuclear magnetic resonance (NMR) spectroscopic studies have implicated the existence of Lewis acid sites on γ-Al_2O_3 and their involvement in catalysis.[5−7] Temperature-programmed desorption (TPD) of 2-propanamine on γ-Al_2O_3 resulted in the amine desorbing molecularly intact and not fragmenting to form ammonia and propene, demonstrating that Brønsted acid sites are not present on the γ-Al_2O_3 surface.[8] Periodic density functional theory (DFT) calculations using a PW91 functional and projector-augmented wave (PAW) methods also show that Lewis acid sites on γ-Al_2O_3(100) adsorb ethanol and water stronger than surface hydroxyl groups.[9]

Early work from Knözinger and Ratnasamy[10] presented structural models for surface structure and site configurations on γ-Al_2O_3, which has subsequently been refined on the basis of more recent computational chemistry studies to elucidate a variety of coordination and hydration states for surface alumina.[11,12] Experimental studies from Wischert et al.[13] also note that thermal treatment of γ-Al_2O_3 resulted in a change in the adsorption energy of N_2 and in the observed activation energy of σ-bonds in H_2 and CH_4 and attribute this to a change in the speciation and number of hydroxyl groups on the alumina surface. The implications of this diversity in coordination and hydration of surface species for catalysis are two-fold: (i) it is likely that under catalytic conditions only a fraction of these Al centers are involved;[14−17] and (ii) parallel reactions may be catalyzed by distinct Al centers. We demonstrate in this research that active sites for unimolecular and bimolecular dehydration of C_2−C_4 alcohols are distinct; however, our studies do not probe the structure of the active sites involved.

Knözinger and co-workers[5,18] proposed an E2-type mechanism for alcohol unimolecular dehydration on γ-Al_2O_3 that

Received: September 26, 2014
Revised: December 1, 2014
Published: December 22, 2014

DOI: 10.1021/cs501471r
ACS Catal. 2015, 5, 602−612

involves concurrent cleavage of C_α−O and C_β−H bonds based on the observed kinetic isotope effect (KIE). For bimolecular dehydration to form ethers, these authors proposed an S_N2-type mechanism involving the reaction of a surface-absorbed alcohol with a surface-bound alkoxide intermediate.[19] Shi and Davis[20] investigated ether formation kinetics on γ-Al_2O_3 at 493 K using 84% (*S*)-(+)/16% (*R*)-(−)-2-butanol and observed that the enantiomer ratio of the ether product was 13% of (*R*,*R*), 13% of (*S*,*S*), and 74% of (*S*,*R*), demonstrating that bimolecular dehydration occurs via an S_N2 pathway. Christiansen et al.[9] in their periodic DFT study of ethanol dehydration on γ-Al_2O_3(100) calculated a lower energy barrier for E2- and S_N2-type mechanisms in comparison with E1 and sequential pathways for unimolecular and bimolecular dehydration, respectively. The mechanistic role of water involves not only the change in coordination/hydration of surface species that consequently results in a change in the number of active centers but also a kinetic role in inhibiting measured rates of dehydration. An empirical description postulating rates of dehydration to vary with $\propto(P_{alcohol}^{1/2})/(P_{alcohol}^{1/2} + bP_{water})$ was proposed by Knözinger et al.;[21] however, the underlying mechanistic basis for this empirical equation remains unclear. Our submission provides a mechanistic basis for the inhibition of observed rates by water and ascribes it to the involvement of dimeric and trimeric surface adsorbate complexes at these low temperatures. The mechanisms that we present are shown to describe the observed pressure dependences of rate for unimolecular and bimolecular dehydration of ethanol, 1-propanol, 2-propanol, and isobutanol at varying alcohol and water pressures. The resulting rate expressions provide a quantitative assessment of rate and equilibrium parameters involved, and from this description, we infer the role of carbon chain length and substitution in determining selectivity and rates for unimolecular and bimolecular dehydration pathways. The first part of this paper reports the similarity of the kinetics and mechanism of parallel unimolecular and bimolecular C_3−C_4 alcohol dehydration to ethanol dehydration. The subsequent discussion compares the assessed rate and equilibrium parameters for different alcohols to show the effects of carbon chain length and substitution on the kinetics of unimolecular and bimolecular dehydration.

2. MATERIALS AND METHODS

2.1. Catalyst Preparation. γ-Al_2O_3 powder (Sasol Catalox 18 HPA-150, BET surface area 141 $m^2\ g^{-1}$, pore volume 0.790 $cm^3\ g^{-1}$) was pressed and sieved to obtain catalyst particles between 180 and 425 μm (40−80 mesh). The reactor bed was formed by mixing the catalyst (0.01−0.2 g) and acid-washed (1 M HNO_3) quartz sand (1.0−1.1 g, 152−422 μm particle size, Acros Organics). The reactor bed was heated while flowing dry air (1.67 $cm^3\ s^{-1}$ at NTP conditions, industrial grade, Matheson Trigas) from ambient temperature to 723 K at 0.0148 K s^{-1} and held at 723 K for 4 h. The bed was subsequently cooled to the reaction temperature (488 K) in flowing dry air (1.67 $cm^3\ s^{-1}$). The catalyst was pretreated before reaction in 2.2 kPa of deionized water diluted with the carrier gas, helium (1.7 $cm^3\ s^{-1}$ at NTP conditions, grade 4.7, Minneapolis Oxygen Company), for 1 h. The bed was regenerated after kinetic experiments using the same procedure as above to remove any remaining alcohol and water in the bed.

2.2. Steady-State Kinetic Measurements of Alcohol Dehydration on γ-Al_2O_3. Steady-state dehydration reactions were carried out in a quartz tube packed bed reactor (10 mm inner diameter) under atmospheric pressure and differential conversion conditions (<10%). A type K thermocouple located on the external surface of the reactor was used to measure the bed temperature, which was retained at reaction temperature (488 K) using a tube furnace (National Electric Furnace FA120 type) and a Watlow temperature controller (96 series).

Liquid pyridine (>99%, Sigma-Aldrich), 1-propanol (≥99.9%, Sigma-Aldrich, 1-PrOH), 1-propanol-OD (99 atom % D, Isotec Inc.), 1-propanol-d_8 (98 atom % D, Sigma-Aldrich), 2-propanol (≥99.5%, Mallinckrodt Chemicals, 2-PrOH), 2-propanol-d_8 (99.5 atom % D, Aldrich), 2-propanol-OD (98 atom % D, Aldrich), isobutanol (99.9%, Fisher Scientific, *i*BuOH), isobutanol-d_9 (C_4D_9OH, 99 atom % D, C/D/N Isotopes Inc.), isobutanol-OD (99.1 atom % D, C/D/N Isotopes Inc.), deuterium oxide (99.9 atom % D, Cambridge Isotope Laboratories, Inc., D_2O), and deionized water components were introduced to heated reactant transfer lines using two separate infusion syringe pumps (KD scientific, KDS100). Alcohol and water mixtures were vaporized at 393 K into a stream of He (1.7−3.2 $cm^3\ s^{-1}$ at NTP conditions) and an internal standard mixture for analysis comprising Ar/CH_4 (10.0% CH_4 and Ar balance, 0.017 $cm^3\ s^{-1}$ at NTP conditions, Minneapolis Oxygen). Partial pressures of components in the feed ($P_{pyridine}$ = 0.02−0.05 kPa, $P_{alcohol}$ = 0.08−7.2 kPa, P_{water} = 0.31−2.2 kPa) were controlled by changing the syringe pump flow rates. Gas lines were resistively heated to maintain temperatures above 343 K and avoid condensation. The reactor effluent was connected via heated transfer lines to an online mass spectrometer (MKS Cirrus 200 quadrupole) and a gas chromatograph (Agilent 6890 N, GC) which was used for all chemical analysis. The GC was equipped with a methylsiloxane capillary column (Agilent HP-5, 50.0 m × 320 μm × 0.52 μm) to separate gaseous species before detection with a flame ionization detector and a packed column (SUPELCO HAY-ESEP R 80/100 mesh packed column, 12 ft) before a thermal conductivity detector. Error bars reported in figures below represent 95% confidence intervals using successive GC injections under the same experimental conditions.

2.3. In Situ Pyridine Titration of Catalytic Ether Formation Sites. C_2−C_3 alcohols (~2.2 kPa) were co-fed with water (1.1 kPa), and isobutanol (~5.0 kPa) was fed to the catalyst bed (0.05, 0.10, and 0.20 g of catalyst) at 488 K. Pyridine (0.02 and 0.05 kPa) was introduced to the reactant flow after steady-state rates of dehydration were observed. The effluent composition was monitored with time-on-stream after introduction of pyridine as a co-feed using an online mass spectrometer. The amount of pyridine to completely deactivate ether synthesis was estimated by linearly extrapolating the initial slope of the deactivation profile, as described in our previous report.[19]

2.4. Parameter Estimation Techniques for Kinetic Modeling. The Athena Visual Studio (v14.2, W.E. Stewart and M. Caracotsios) statistical software package with Bayesian statistical estimation techniques was used to optimize kinetic parameters. Replicates are defined as experimental measurements obtained when the alcohol and water pressures are the same. These measurements represent a collection of independent experiments that involved keeping either the alcohol or water pressure constant while varying the other, as discussed in section 3.3.

DOI: 10.1021/cs501471r
ACS Catal. 2015, 5, 602−612

3. RESULTS AND DISCUSSION

3.1. Effects of Water Pretreatment of γ-Al_2O_3 on C_3–C_4 Alcohol Dehydration Rates. The synthesis rates of olefin and ether from 1-PrOH, 2-PrOH, and *i*BuOH dehydration at 488 K on water-exposed γ-Al_2O_3 (2.2 kPa of water at 488 K for 1 h) samples were lower than the rates on non-exposed γ-Al_2O_3 samples; catalytic rates for samples exposed to water could be regenerated after thermal treatment (1.67 cm^3 s^{-1} of dry air at 723 K for 4 h), as shown in Table 1. These effects of water reflect the hydration/coordination of surface alumina as discussed in section 1. A decrease in rates and regeneration upon thermal treatment were also observed for ethanol (EtOH) dehydration[19] and show that water molecules irreversibly adsorb onto a fraction of the catalytic sites, which causes deactivation with time-on-stream at this reaction temperature. Catalyst samples, therefore, were pretreated with water before introduction of alcohol reactants to deactivate this fraction of sites and run under steady-state conditions.

Table 1. Olefin and Ether Synthesis Rates for 1-PrOH, 2-PrOH, and *i*BuOH Dehydration with 2.5 kPa Alcohol Partial Pressures at 488 K on γ-Al_2O_3[a]

	olefin synthesis rate (10^{-6} mol g_{cat}^{-1} s^{-1})			ether synthesis rate (10^{-6} mol g_{cat}^{-1} s^{-1})		
catalyst sample	1-PrOH	2-PrOH	*i*BuOH	1-PrOH	2-PrOH	*i*BuOH
no water pretreatment	4.99	31.4	5.48	5.12	2.54	0.170
water pretreated	1.97	21.5	2.59	3.77	1.75	0.121
regenerated	5.30	37.8	5.61	5.72	2.94	0.176

[a]With 0.02 g for 1-PrOH and 2-PrOH and 0.01 g for *i*BuOH, under total gas flow rate of 3.4 cm^3 s^{-1} for a catalyst sample which was not pretreated with water, a catalyst sample which was pretreated with 2.2 kPa of water for 1 h, and a regenerated water-pretreated sample with drying air (1.67 cm^3 s^{-1}) at 723 K for 4 h.

3.2. Kinetic Isotope Effects for C_3–C_4 Alcohol Dehydration. Kinetic isotope effects probing the involvement of C–H and O–H bonds in kinetically relevant steps for unimolecular and bimolecular dehydration of 1-PrOH, 2-PrOH, and *i*BuOH were measured. The rates of unimolecular and bimolecular dehydration using protium-form C_3–C_4 alcohols relative to the rates of dehydration using deuterated reactants such as C_3D_7OD (1-PrOH-d_8), C_3H_7OD (1-propanol-OD), $CD_3CD(OD)CD_3$ (2-PrOH-d_8), $CH_3CH(OD)CH_3$ (2-propanol-OD), C_4D_9OH (*i*BuOH-d_9), and C_4H_9OD (isobutanol-OD) (r_H/r_D) at 488 K are presented in Tables 2–4.

No significant effect (Tables 2–4) on the rate of bimolecular dehydration is observed using any deuterated reactant, demonstrating that the rate-determining step (RDS) of bimolecular dehydration does not involve the cleavage of a C–H or O–H bond, similar to what has previously been reported for EtOH dehydration.[19] The RDS for dipropyl ether (DPE), diisopropyl ether (DiPE), and diisobutyl ether (DiBE) formation, therefore, involves C_α–O or Al–O bond breakage. The rates of unimolecular dehydration using 1-propanol-OD, 2-propanol-OD, and isobutanol-OD as reactants are not significantly different (Tables 2–4), suggesting that O–H bond cleavage is not the kinetically relevant step in olefin formation. A primary kinetic isotope effect was observed for olefin formation when using 1-PrOH-d_8, 2-PrOH-d_8, and *i*BuOH-d_9 as reactants, confirming that C_β–H bond cleavage is the RDS for unimolecular dehydration. These observations and conclusions are in agreement with prior reports by Knözinger and Scheglila[18] for 2-butanol, *tert*-butyl alcohol, and *i*BuOH dehydration at temperatures similar to those used in this research (393–483 K) and by Shi et al.[22] for *tert*-butyl alcohol dehydration on γ-Al_2O_3 over the temperature range of 458–493 K.

Table 2. Measured Kinetic Isotope Effects for Propene and DPE Synthesis at 488 K for the Dehydration of 1-PrOH-d_8 and 1-Propanol-OD[a]

	reactant	
product	1-PrOH-d_8	1-propanol-OD
propene KIE (r_H/r_D)	2.03 ± 0.25	0.90 ± 0.09
DPE KIE (r_H/r_D)	0.86 ± 0.08	0.88 ± 0.05

[a]Over γ-Al_2O_3 with 0.7 kPa of alcohol and 0.5 kPa of water (H_2O for 1-PrOH and D_2O for 1-PrOH-d_8 and 1-propanol-OD) at 3.4 cm^3 s^{-1} of total flow rate.

Table 3. Measured Kinetic Isotope Effects for Propene and DiPE Synthesis at 488 K for the Dehydration of 2-PrOH-d_8 and 2-Propanol-OD[a]

	reactant	
product	2-PrOH-d_8	2-propanol-OD
propene KIE (r_H/r_D)	2.18 ± 0.12	1.17 ± 0.04
DiPE KIE (r_H/r_D)	0.82 ± 0.02	1.06 ± 0.02

[a]Over γ-Al_2O_3 with 0.6 kPa of alcohol and 0.7 kPa of water (H_2O for 2-PrOH and D_2O for 2-PrOH-d_8 and 2-propanol-OD) at 3.4 cm^3 s^{-1} of total flow rate.

Table 4. Measured Kinetic Isotope Effects for Isobutene and DiBE Synthesis at 488 K for the Dehydration of *i*BuOH-d_9 and Isobutanol-OD[a]

	reactant	
product	*i*BuOH-d_9	isobutanol-OD
isobutene KIE (r_H/r_D)	1.97 ± 0.11	1.09 ± 0.06
DiBE KIE (r_H/r_D)	1.00 ± 0.06	1.05 ± 0.06

[a]Over γ-Al_2O_3 with 0.7 kPa of alcohol and 0.3 kPa of water (H_2O for *i*BuOH and D_2O for *i*BuOH-d_9 and isobutanol-OD) at 3.4 cm^3 s^{-1} of total flow rate.

3.3. Kinetics and Mechanism of Alcohol Dehydration. The rates and selectivity of 1-PrOH, 2-PrOH, and *i*BuOH dehydration were measured at varying alcohol and water partial pressures to assess the kinetics of parallel unimolecular and bimolecular dehydration mechanisms.

3.3.1. Kinetics and Mechanism of Unimolecular Dehydration. 3.3.1.1. Kinetics and Mechanism of 1-PrOH Unimolecular Dehydration. The propene formation rate when co-feeding 1-PrOH and water at 488 K showed negative order dependences on 1-PrOH and water pressure, as shown in Figure 1 (1-PrOH partial pressure = 0.4–7.3 kPa and water partial pressure = 0.3–2.2 kPa). The reaction order in 1-PrOH (between −0.2 and 0) changes with water pressure and asymptotically lines out to zero at high water pressure (~1.1 kPa), suggesting that inhibition of unimolecular dehydration rates by water is a consequence of 1-PrOH/water dimers on the surface. Propene synthesis rate was observed to have a water pressure dependence less than −1 (−1.3) at low 1-PrOH partial pressure (~0.70 kPa) and high water partial pressure (>2 kPa), as shown in Supporting Information Figure S1,

DOI: 10.1021/cs501471r
ACS Catal. 2015, 5, 602–612

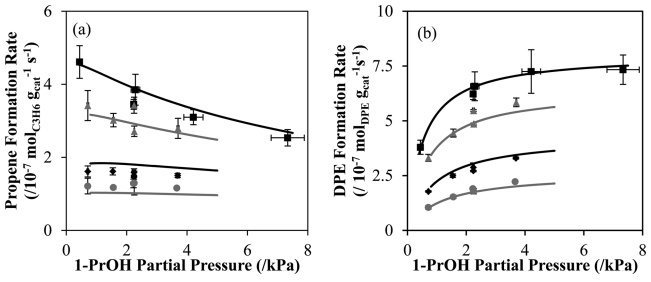

Figure 1. (a) Propene and (b) DPE formation rate for 1-PrOH dehydration at 488 K on γ-Al_2O_3 as a function of 1-PrOH partial pressure with (black square) 0.32, (gray triangle) 0.55, (black diamond) 1.1, and (gray circle) 2.2 kPa water co-feeds (total gas flow rate = 3.4 cm^3 s^{-1}). The solid line represents the model fits to eqs 2 and 4 for (a) and (b), respectively.

suggesting the existence of water dimers on the surface that inhibit unimolecular dehydration rates. The negative order in 1-PrOH reveals that 1-PrOH dimers exist on the surface and also inhibit the formation of propene. 1-PrOH monomers are expected to be prominent on the catalyst surface as they are involved in the RDS for unimolecular 1-PrOH dehydration. A kinetic model that considers 1-PrOH monomers, 1-PrOH dimers, 1-PrOH/water dimers, water monomers, and water dimers as surface species that competitively occupy surface sites can consistently describe these observations as discussed below.

The alcohol monomer involved in the RDS of olefin formation can be either a physisorbed molecular complex[9] or a chemisorbed alkoxide. Pines and Haag[23] observed that both 1-butanol dehydration and 1-butene double bond isomerization showed a nearly identical *cis*/*trans* ratio (~2) for 2-butene synthesis on alumina, indicating that alcohol dehydration is accompanied by fast adsorption and isomerization of the olefin. The *cis*/*trans* ratio for 2-butanol dehydration and 2-butene isomerization on alumina was also observed to be identical (~4.3). These results suggest that the intermediates for alcohol dehydration and olefin double bond isomerization are the same and that desorption of these intermediates is the rate-limiting step. Macht et al.[24] also observed that the *cis*/*trans* ratio of 2-butene is nearly identical for 2-butanol dehydration and 1-butene isomerization on polyoxometalate catalysts. The authors concluded that surface alkoxide species dissociated from alcohols are common intermediates between the two reactions. When γ-Al_2O_3 was exposed to EtOH (308−573 K), IR spectra of the alumina contained a band similar to $Al(OCH_2CH_3)_3$, suggesting the existence of alkoxide species.[25] Chemical shifts representing alkoxide species were also observed in ^{13}C solid-state NMR measurements of γ-Al_2O_3 exposed to ^{13}C-labeled propene, *n*-butene, and isobutene (63 and 79 ppm, 69 and 74 ppm, and 67 ppm, respectively).[26] Knözinger and Scheglila[18] considered concurrent C−H and C−OH bond cleavage in an adsorbed alcohol on γ-Al_2O_3 and postulated a mechanism that does not consider surface alkoxide species. Recent density functional theory calculations reported by Christiansen et al.[9] also show that molecularly intact alcohol precursors mediate unimolecular dehydration on the (100) surface of γ-Al_2O_3 with a lower barrier than alkoxide precursors. Kinetically, these two postulates are indistinguishable except for the appearance of an equilibrium parameter for alcohol dissociation, K_d (Step 2, Scheme 1) in the rate expression. K_d cannot be explicitly assessed from the kinetic studies that we report and always appears in the rate expression accompanied by other

Scheme 1. 1-Propoxide Desorption-Limited Mechanism for Propene Formation from 1-PrOH Dehydration

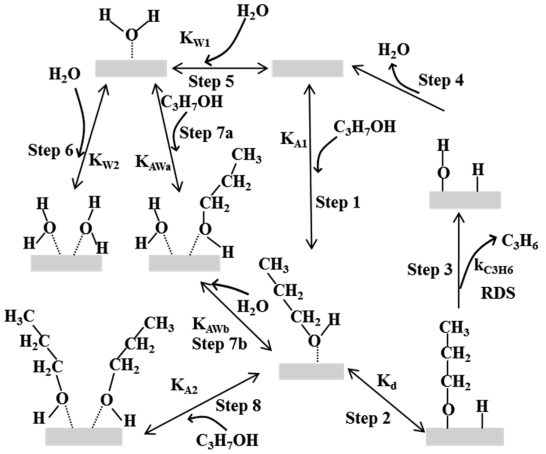

equilibrium constants. We postulate the existence of alkoxide species (Scheme 1) and the RDS to involve C−H bond cleavage in this surface intermediate; however, as pointed out above, an equivalent model considering C−H bond cleavage from molecular alcohol precursors to be the RDS would result in a kinetically indistinguishable model. The mechanism proposed in Scheme 1 comprising surface propoxide species, water, and 1-PrOH monomers and dimers and 1-PrOH/water dimers can explain the measured kinetic dependences for propene synthesis. All intermediates are considered to be in quasi-equilibrium before the RDS. A 1-PrOH molecule adsorbs onto γ-Al_2O_3 (Step 1, Scheme 1) and subsequently dissociates to form a 1-propoxide species and an adsorbed hydrogen atom (Step 2, Scheme 1). The 1-propoxide species desorbs from the surface by β-hydrogen elimination and is converted to a propene molecule and a hydroxyl group in the RDS (Step 3, Scheme 1). The hydroxyl group and a hydrogen atom on the surface desorb to form a water molecule, which completes the catalytic cycle and regenerates the catalytic surface (Step 4, Scheme 1). The adsorption of a water molecule (Step 5, Scheme 1) and the subsequent adsorption of a second water molecule or a 1-PrOH molecule forming either a water dimer (Step 6, Scheme 1) or a 1-PrOH/water dimer (Step 7a, Scheme 1), respectively, can inhibit the catalytic rate. A water molecule can also adsorb onto a surface-bound 1-PrOH molecule to form the 1-PrOH/water dimer (Step 7b, Scheme 1). Steps 7a and 7b, which both form a 1-PrOH/water dimer, however, cannot be kinetically distinguished. The 1-PrOH dimer species formed from the adsorption of an additional 1-PrOH molecule onto the 1-PrOH adsorbed site can also inhibit propene formation (Step 8, Scheme 1).

The propene formation rate (r_{olefin}) derived from the mechanism depicted in Scheme 1 is shown in eq 1.

$$r_{olefin} = (k_{olefin}K_dK_{A1}P_{alcohol})/(1 + K_dK_{A1}P_{alcohol} + K_{W1}P_{water} + (K_{W1}K_{AWa} + K_{A1}K_{AWb})P_{alcohol}P_{water} + K_{A1}K_{A2}P^2_{alcohol} + K_{W1}K_{W2}P^2_{water}) \quad (1)$$

where k_{olefin} is the rate constant of the RDS and K_d, K_{A1}, K_{A2}, K_{W1}, K_{W2}, and K_{AW} are equilibrium constants for the dissociation of adsorbed 1-PrOH to form 1-propoxide species, formation of adsorbed 1-PrOH, 1-PrOH dimer, adsorbed water, water dimer, and 1-PrOH/water dimer, respectively, on

DOI: 10.1021/cs501471r
ACS Catal. 2015, 5, 602−612

the surface. K_{AWa} and K_{AWb} are equilibrium constants for the two indistinguishable routes to form a 1-PrOH/water dimer.

The observed negative order dependence of propene formation rates on water and 1-PrOH pressures and the observed kinetic isotope effect implying the involvement of alkoxide species in the RDS indicate that the 1-propoxide group, 1-PrOH/water dimers, 1-PrOH dimers, and water dimers are the dominant surface species, and a simplified rate expression shown in eq 2 can be derived from eq 1.

$$r_{olefin} = \left(k_{olefin}P_{alcohol}\right)\Big/\left(P_{alcohol} + \frac{K'_{AW}}{K_{A1}K_d}P_{alcohol}P_{water} + \frac{K_{A1}K_{A2}}{K_{A1}K_d}P^2_{alcohol} + \frac{K_{W1}K_{W2}}{K_{A1}K_d}P^2_{water}\right) \quad (2)$$

where K'_{AW} represents the sum of the equilibrium constants for two indistinguishable routes for the formation of 1-PrOH/water dimer species ($K'_{AW} = K_{W1}K_{AWa} + K_{A1}K_{AWb}$). Based on eq 2, a nonlinear parameter estimation of the propene formation rate data was performed using Athena Visual Studio (v14.2, W.E. Stewart and M. Caracotsios) to determine rate and equilibrium parameters shown in eq 2. The optimized parameters are shown in Table 5, and the model fits to eq 2 are shown in Figure 1. Analysis of residual error in the kinetic model is reported in Supporting Information, Figures S3–S5.

Table 5. Estimated Kinetic Parameters for Unimolecular Dehydration of 1-PrOH on γ-Al_2O_3 at 488 K Using the Model Presented in Equation 2 and Data from Figure 1

parameter	$k_{C_3H_6}$ (10^{-6} $mol_{C_3H_6}$ g_{cat}^{-1} s^{-1})	$(K'_{AW})/(K_{A1}K_d)$ (kPa^{-1})	$(K_{A1}K_{A2})/(K_{A1}K_d)$ (kPa^{-1})	$(K_{W1}K_{W2})/(K_{A1}K_d)$ (kPa^{-1})
estimated value	1.20	4.49	0.271	0.292

The much larger value of $(K'_{AW})/(K_{A1}K_d)$, 4.49, compared to $(K_{A1}K_{A2})/(K_{A1}K_d)$, 0.271, and $(K_{W1}K_{W2})/(K_{A1}K_d)$, 0.292, suggests that 1-PrOH/water dimers predominantly occupy the surface at the alcohol and water pressures used in this study and that the concentrations of 1-PrOH dimers and water dimers are low. This model consistently explains the negative order dependence of the reaction rate on $P_{1\text{-PrOH}}$ (between −0.2 and 0) and the asymptotic convergence of the order in $P_{1\text{-PrOH}}$ to zero as P_{water} increases.

3.3.1.2. Kinetics and Mechanism of 2-PrOH Unimolecular Dehydration. The propene formation rate from 2-PrOH and water co-fed at 488 K showed zero order dependence on 2-PrOH partial pressure and negative order dependence on water partial pressure as shown in Figure 2 (2-PrOH partial pressure = 2.2–7.2 kPa and water partial pressure = 0.33–2.1 kPa). A slight positive dependence on 2-PrOH at low partial pressures (≤2 kPa) was observed. These observations corroborate the inference that water and 2-PrOH/water dimers inhibit unimolecular dehydration. The less than −1 dependence of propene formation rates on water partial pressures at low 2-PrOH partial pressure (~0.65 kPa) and high water partial pressure (>2 kPa) ($r_{C_3H_6} \propto P_{H_2O}^{-1.34}$), as shown in Figure S1, confirms the existence of water dimers on the surface. The reaction order in 2-PrOH is slightly negative at high 2-PrOH pressure (≥2 kPa) and low water pressure (~0.33 kPa), which suggests inhibition of unimolecular dehydration rates by 2-PrOH dimers on the surface. 2-PrOH monomers are expected to exist in the RDS because the olefin is formed from unimolecular dehydration. The model for 1-PrOH, Scheme 1, and eq 1 can also explain the mechanism of 2-PrOH unimolecular dehydration. The 2-propoxide species, 2-PrOH/water dimers, 2-PrOH dimers, and water dimers are identified as dominant surface species from experimental rate dependences, and therefore, a surrogate of eq 1 for 2-PrOH can be simplified to eq 2. The parameters and the model fit of this equation are shown in Table 6 and Figure 2, respectively.

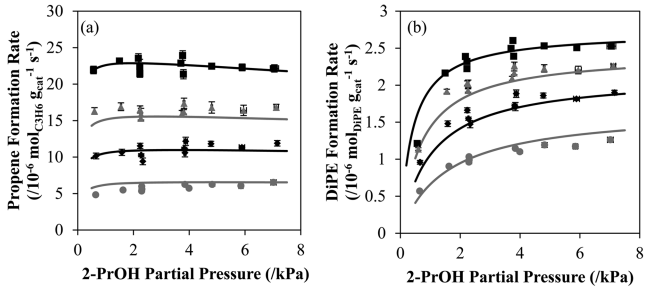

Figure 2. (a) Propene and (b) DiPE formation rate for 2-PrOH dehydration at 488 K on γ-Al_2O_3 as a function of 2-PrOH partial pressure with (black square) 0.33, (gray triangle) 0.65, (black diamond) 1.1, and (gray circle) 2.1 kPa water co-feeds (total gas flow rate = 3.4 cm^3 s^{-1}). The solid line represents the model fits to eqs 2 and 4 for (a) and (b), respectively.

Table 6. Estimated Kinetic Parameters for Unimolecular Dehydration of 2-PrOH on γ-Al_2O_3 at 488 K Using the Model Presented in Equation 2 and Data from Figure 2

parameter	$k_{C_3H_6}$ (10^{-5} $mol_{C_3H_6}$ g_{cat}^{-1} s^{-1})	$(K'_{AW})/(K_{A1}K_d)$ (kPa^{-1})	$(K_{A1}K_{A2})/(K_{A1}K_d)$ (kPa^{-1})	$(K_{W1}K_{W2})/(K_{A1}K_d)$ (kPa^{-1})
estimated value	4.13	2.33	0.0163	0.371

The high value of $(K'_{AW})/(K_{A1}K_d)$, 2.33, compared to $(K_{A1}K_{A2})/(K_{A1}K_d)$, 0.0163, and $(K_{W1}K_{W2})/(K_{A1}K_d)$, 0.371, shows that 2-PrOH/water dimers are the dominant surface species under the reaction conditions employed, similar to the observation noted above for 1-PrOH/water dimers being dominant for 1-PrOH dehydration. The much smaller value of $(K_{A1}K_{A2})/(K_{A1}K_d)$ in reference to other adsorption parameters suggests that 2-PrOH dimers are scarce and explains the weaker negative dependence on alcohol partial pressure for 2-PrOH compared to 1-PrOH. This model explains the unimolecular dehydration rate dependences on 2-PrOH and water partial pressures. The rate constant of propene formation for 2-PrOH dehydration is 4.13×10^{-5} $mol_{propene}$ g_{cat}^{-1} s^{-1}, which is an order of magnitude larger than the rate constant for 1-PrOH dehydration, 1.20×10^{-6} $mol_{propene}$ g_{cat}^{-1} s^{-1}. The increased rate constant with C_α substitution as noted for 2-PrOH in comparison with 1-PrOH, and thus, carbocation stability is indicative of a carbocation-like transition state.[8,27] The difference in reaction rate constants among different alcohols will be discussed further in section 3.5.

3.3.1.3. Kinetics and Mechanism of iBuOH Unimolecular Dehydration. The isobutene formation rate when feeding *i*BuOH and water mixtures at 488 K is shown in Figure 3 (*i*BuOH partial pressure = 0.08–7.3 kPa and water partial pressure = 0.34–4.5 kPa). The isobutene synthesis rate decreased as water partial pressure increased. At low *i*BuOH partial pressure (≤1 kPa), the isobutene synthesis rate shows

DOI: 10.1021/cs501471r
ACS Catal. 2015, 5, 602–612

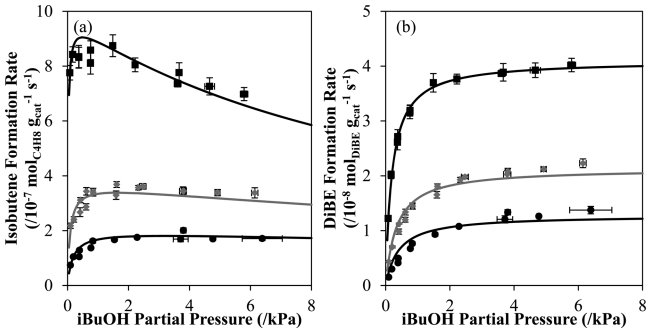

Figure 3. (a) Isobutene and (b) DiBE formation rate for *i*BuOH dehydration at 488 K on γ-Al_2O_3 as a function of *i*BuOH partial pressure with (black square) 0.34, (gray diamond) 1.1, and (black circle) 2.3 kPa water co-feeds (total gas flow rate = 3.4 $cm^3\ s^{-1}$). The solid line represents the model fits to eqs 2 and 4 for (a) and (b), respectively.

positive dependence on *i*BuOH pressure. At higher *i*BuOH partial pressures (>1 kPa), the reaction order in *i*BuOH is negative at low water pressure (~0.34 kPa) and asymptotically lines out to zero as water pressure increases (>1.1 kPa). These observations show that water and *i*BuOH/water dimers inhibit isobutene formation. The observed negative dependence of unimolecular dehydration rates on *i*BuOH confirms inhibition by *i*BuOH dimers on the surface. Similar to 1- and 2-PrOH, water pressure dependences less than −1 were observed at high water and low *i*BuOH partial pressures, suggesting that water dimers are formed and inhibit unimolecular dehydration. *i*BuOH monomers are involved in the RDS as observed in other unimolecular C_2−C_3 alcohol dehydration mechanisms. The dimer inhibition model proposed by DeWilde et al.,[19] therefore, rigorously describes the observed reaction order dependences not only for EtOH but also for longer and more substituted C_3−C_4 alcohols. Equation 1 was modified to eq 2 with dominant isobutoxide species, *i*BuOH/water dimers, *i*BuOH dimers, and water dimers. The estimated parameters are shown in Table 7, and the model fit is shown in Figure 3.

Table 7. Estimated Kinetic Parameters for Unimolecular Dehydration of *i*BuOH on γ-Al_2O_3 at 488 K Using the Model Presented in Equation 2 and Data from Figure 3

parameter	$k_{C_4H_8}$ (10^{-6} $mol_{C_4H_8}\ g_{cat}^{-1}\ s^{-1}$)	$(K'_{AW})/(K_{A1}K_d)$ (kPa^{-1})	$(K_{A1}K_{A2})/(K_{A1}K_d)$ (kPa^{-1})	$(K_{W1}K_{W2})/(K_{A1}K_d)$ (kPa^{-1})
estimated value	3.29	6.86	0.282	0.577

*i*BuOH/water dimer dominates the γ-Al_2O_3 surface at the conditions employed as inferred from the assessed values of adsorption parameters: $(K'_{AW})/(K_{A1}K_d)$, 6.86, $(K_{A1}K_{A2})/(K_{A1}K_d)$, 0.282, and $(K_{W1}K_{W2})/(K_{A1}K_d)$, 0.577. *i*BuOH dimers are nearly absent from the surface at these conditions. The isobutene formation rate dependences on *i*BuOH and water partial pressures are explained by this model. The rate constant of isobutene formation is 3.29×10^{-6} $mol_{isobutene}\ g_{cat}^{-1}\ s^{-1}$; this value is similar to the rate constant of propene formation from 1-PrOH because both alcohols have primary C_α. The electron-donating methyl groups of *i*BuOH will stabilize the carbocation-like transition state to a greater degree than those of 1-PrOH, which results in a slightly larger rate constant for isobutene formation. The comparison of reaction rate constants among different alcohols will be discussed in section 3.5.

3.3.2. Kinetics and Mechanism of Bimolecular Dehydration. 3.3.2.1. Kinetics and Mechanism of 1-PrOH Bimolecular Dehydration. The measured rates of DPE formation increase with increasing 1-PrOH pressure and asymptotically line out at high 1-PrOH pressure (~4.2 kPa) at 488 K, as shown in Figure 1 (1-PrOH partial pressure = 0.4−7.3 kPa and water partial pressure = 0.3−2.2 kPa). Ether formation occurs via an S_N2-type bimolecular dehydration step[5,20] as discussed in section 1, so 1-PrOH dimers on the surface are considered to be involved in the RDS. The DPE synthesis rate asymptotically lined out and showed negative order (nearly −1) for water at high 1-PrOH pressure (~4.2 kPa), which can be explained by the inhibition of 1-PrOH dimer/water monomer trimers on the surface of γ-Al_2O_3; the involvement of trimers is inferred from the formation rates of DPE asymptotically lining out to different values at high 1-PrOH pressures depending on the water pressure (Figure 1). The inhibition of water and positive dependence on 1-PrOH pressure at low partial pressures of 1-PrOH (<2.3 kPa) can be explained by the existence of 1-PrOH/water dimers. A kinetic model, similar to that for propene formation discussed above, with 1-PrOH monomers, 1-PrOH dimers, water monomers, water dimers, 1-PrOH/water dimers, and 1-PrOH dimer/water monomer trimers is proposed and discussed below.

A 1-PrOH molecule adsorbs on the γ-Al_2O_3 surface (Step 1, Scheme 2) followed by co-adsorption of another 1-PrOH molecule (Step 2, Scheme 2). Subsequent dehydration of the 1-PrOH dimer forms DPE and water while regenerating the catalytic site in the RDS (Step 3, Scheme 2). This step, however, is assumed to comprise several fundamental steps, some of which are not kinetically observable. A water molecule can nondissociatively adsorb on the active site (Step 4, Scheme 2) and, following adsorption of a second water molecule or a 1-PrOH molecule, forms either a water dimer (Step 5, Scheme 2) or a 1-PrOH/water dimer (Step 6a, Scheme 2), respectively, capable of inhibiting DPE synthesis. The co-adsorption of a water molecule with an adsorbed 1-PrOH species could also form 1-PrOH/water dimers as discussed in section 3.3.1 (Step 6b, Scheme 2). The existence of only monomeric and dimeric 1-PrOH and water species is, however, inconsistent with the asymptotic behavior of ether synthesis rates at high alcohol pressures. A mechanism that considers only 1-PrOH/water and water dimers to inhibit rates would predict that DPE synthesis rates at high 1-PrOH pressures asymptotically converge to a single value, independent of water pressure. Experimental observations contradict this model (for 1-PrOH, 2-PrOH, and *i*BuOH as shown below) and lead us to postulate another inhibiting species, a 1-PrOH dimer/water monomer trimer which is formed by addition of 1-PrOH to 1-PrOH/water dimer (Step 7a, Scheme 2) or water to 1-PrOH dimer (Step 7b, Scheme 2). A trimeric species as postulated above does not require each of the three species to interact with the active site; instead, it may involve, for example, the interaction/adsorption of water with a surface-adsorbed alcohol dimer via hydrogen bonding. This surface-bound complex comprising two molecules of the alcohol and a water molecule would therefore be unreactive for bimolecular dehydration and would describe the observed inhibition of reaction rates by water.

Equation 3 represents the DPE formation rate equation (r_{ether}) derived from the proposed mechanism in Scheme 2 with k_{ether} as the rate constant of the RDS.

DOI: 10.1021/cs501471r
ACS Catal. 2015, 5, 602−612

Scheme 2. 1-PrOH Dimer/Water Monomer Trimer Inhibition Mechanism for DPE Formation from 1-PrOH Dehydration

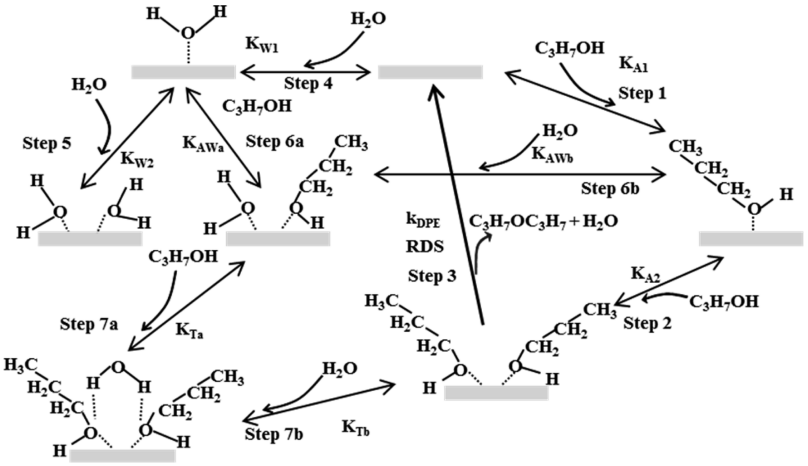

$$r_{ether} = (k_{ether}K_{A1}K_{A2}P^2_{alcohol}) / ([1 + K_{A1}P_{alcohol} + K_{W1}P_{water} + (K_{W1}K_{AWa} + K_{A1}K_{AWb})P_{alcohol}P_{water} + K_{A1}K_{A2}P^2_{alcohol} + K_{W1}K_{W2}P^2_{water} + \{(K_{W1}K_{AWa} + K_{A1}K_{AWb})K_{Ta} + K_{A1}K_{A2}K_{Tb}\} P^2_{alcohol}P_{water}]) \quad (3)$$

The 1-PrOH dimer/water monomer trimer term in the denominator explains the concurrent zero order dependence on 1-PrOH pressure and the inverse order dependence on water pressure observed experimentally at high 1-PrOH partial pressures (>4.2 kPa). The positive order in 1-PrOH and the negative order dependence on water pressures observed at low 1-PrOH pressures (<2.3 kPa) mandate the existence of 1-PrOH/water dimers. Equation 3 was simplified to eq 4 based on the observed pressure dependences of DPE synthesis rates on 1-PrOH and water pressures to include only 1-PrOH dimers, 1-PrOH/water dimers, and 1-PrOH dimer/water monomer trimers as the prominent surface species.

$$r_{ether} = \frac{k_{ether}P^2_{alcohol}}{P^2_{alcohol} + \frac{K'_{AW}}{K_{A1}K_{A2}}P_{alcohol}P_{water} + \frac{K'_{T}}{K_{A1}K_{A2}}P^2_{alcohol}P_{water}} \quad (4)$$

where K'_{AW} and K'_{T} represent the sum of the equilibrium constants of two indistinguishable routes for the formation of 1-PrOH/water dimers and 1-PrOH dimer/water monomer trimers ($K'_{AW} = K_{W1}K_{AWa} + K_{A1}K_{AWb}$ and $K'_{T} = (K_{W1}K_{Awa} + K_{A1}K_{AWb})K_{Ta} + K_{A1}K_{A2}K_{Tb}$). Nonlinear parameter estimation of the DPE synthesis rate data to calculate rate and equilibrium parameters shown in eq 4 resulted in the optimized parameters shown in Table 8 and a fit of the data shown in Figure 1. The similar values of $(K'_{AW})/(K_{A1}K_{A2})$ and $(K'_{T})/(K_{A1}K_{A2})$ imply that DPE synthesis rates are independent of 1-PrOH pressure at high 1-PrOH pressure (Figure 1).

Table 8. Estimated Kinetic Parameters of DPE Formation from 1-PrOH on γ-Al_2O_3 at 488 K Using the Model Presented in Equation 4 and Data from Figure 1

parameter	k_{DPE} (10^{-6} mol_{DPE} g_{cat}^{-1} s^{-1})	$(K'_{AW})/(K_{A1}K_{A2})$	$(K'_{T})/(K_{A1}K_{A2})$ (kPa^{-1})
estimated value	1.27	2.50	1.79

3.3.2.2. Kinetics and Mechanism of 2-PrOH and iBuOH Bimolecular Dehydration. DiPE and DiBE synthesis rates show similar trends as DPE synthesis. Ether formation rates asymptotically converge to different values at high alcohol pressure (>4 kPa) and concurrently show a negative order dependence (nearly −1) on the water partial pressure. A positive dependence on alcohol pressure and negative dependence on water pressure at low alcohol pressures (<2 kPa) is also observed. The mechanism in Scheme 2 and the rate equation derived for bimolecular dehydration (eq 4) accurately describe ether synthesis for 1-PrOH, 2-PrOH, and *i*BuOH. The optimized parameters for DiPE and DiBE are shown in Tables 9 and 10, respectively. The significantly lower rate constant for

Table 9. Estimated Kinetic Parameters of DiPE formation from 2-PrOH on γ-Al_2O_3 at 488 K Using the Model Presented in Equation 4 and Data from Figure 2

parameter	k_{DiPE} (10^{-6} mol_{DiPE} g_{cat}^{-1} s^{-1})	$(K'_{AW})/(K_{A1}K_{A2})$	$(K'_{T})/(K_{A1}K_{A2})$ (kPa^{-1})
estimated value	3.08	1.36	0.403

Table 10. Estimated Kinetic Parameters of DiBE Formation from *i*BuOH on γ-Al_2O_3 at 488 K Using the Model Presented in Equation 4 and Data from Figure 3

parameter	k_{DiBE} (10^{-8} mol_{DiBE} g_{cat}^{-1} s^{-1})	$(K'_{AW})/(K_{A1}K_{A2})$	$(K'_{T})/(K_{A1}K_{A2})$ (kPa^{-1})
estimated value	6.82	0.962	1.93

DiBE formation (6.82×10^{-8} mol_{DiBE} g_{cat}^{-1} s^{-1}) compared to that for DPE (1.27×10^{-6} mol_{DPE} g_{cat}^{-1} s^{-1}) or DiPE formation (3.08×10^{-6} mol_{DiPE} g_{cat}^{-1} s^{-1}) suggests that the bulky alkyl group in *i*BuOH causes steric hindrance during S_N2 ether formation reactions. The consequences of this difference in bimolecular dehydration reaction rate constants on olefin and ether selectivity will be discussed in section 3.5.

Rep et al.[28] measured IR spectra of adsorbed methanol on sodium-exchanged zeolite X (Na-X, silicon/aluminum ratio of 1.3) at 308 K and observed maxima at 3485 and 3354 cm^{-1}. These observations led the authors to postulate the existence of hydrogen bonding networks between hydroxyl groups in

DOI: 10.1021/cs501471r
ACS Catal. 2015, 5, 602−612

Scheme 3. Two Distinct Sites Mechanism for DPE Formation from 1-PrOH Dehydration

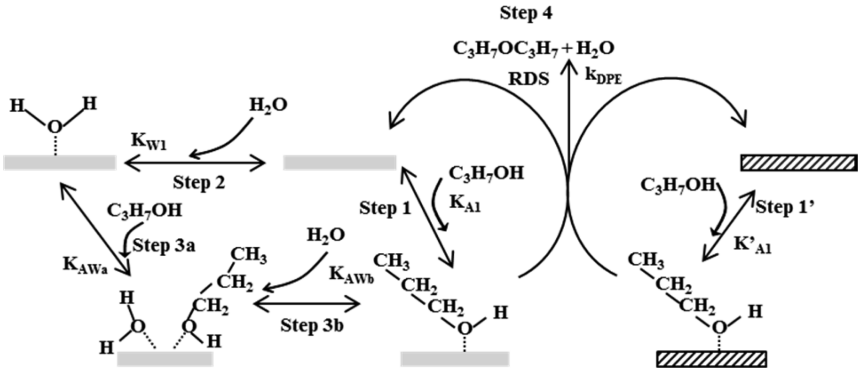

methanol and oxygen atoms in the zeolite structure (3485 cm^{-1}) and between adsorbed methanol molecules on adjacent Na cations. They proposed that methanol molecules in the Faujasite cage form complexes with more than three molecules stabilized by hydrogen bonding with other alcohols and zeolite surface oxygen atoms and by interactions between Na cations and the oxygen atom in methanol. Schenkel et al.[29] measured IR spectra of adsorbed C_2-C_4 alcohols (EtOH, 1-PrOH, 1-butanol) on Na-X at 308 K and also observed bands at ~3350 cm^{-1}, similar to what was observed by Rep et al. for methanol adsorption, which led the authors to suggest that trimeric or larger complexes are formed upon adsorption of C_1-C_4 alcohols onto acidic zeolites at low temperatures. Inelastic neutron scattering spectra in this study showed a broad band for the vibrational mode of the alcohol hydroxyl group (a maximum at 715 cm^{-1} for EtOH and 690 cm^{-1} for 1-PrOH and 1-butanol), also indicating the formation of a hydrogen bond network. Wang et al.[30] calculated trajectories of water, methanol, and EtOH in bulk solution and microporous silicalite-1 using configurational bias Monte Carlo in the Gibbs ensemble at 298 K and molecular dynamics at 300−350 K and inferred from these trajectories that clusters of water, methanol, and EtOH are formed in the zeolite framework. On the same lines, we postulate that alcohol dimer/water monomer trimers exist on γ-Al_2O_3 at these low-temperature conditions.

Equation 4 can be rewritten in the form of eq 5 which considers the surface to comprise two distinct sites (Scheme 3): one site which is predominantly occupied by the alcohol and the other site being occupied by alcohol, water, and alcohol/water dimers.

$$r_{ether} = \frac{k_{ether} P_{alcohol}}{P_{alcohol} + \frac{K_{W1}}{K_{A1}} P_{water} + \frac{K'_{AW}}{K_{A1}} P_{alcohol} P_{water}} \times \frac{P_{alcohol}}{P_{alcohol}} \quad (5)$$

Adsorbed water and alcohol/water dimers inhibit observed bimolecular dehydration rates for this model. Shi and Davis[20] when studying the dehydration of secondary alcohols on γ-Al_2O_3 proposed that one alcohol molecule should be in alkoxide form and act as a nucleophile while the other alcohol molecule is physisorbed and acts as an electrophile for the S_N2 reaction to form an ether, which requires two adjacent sites. Following Shi and Davis, a two-site model consistent with the observed asymptotic behavior of ether synthesis rates would involve the formation of alkoxide species on one site and the competitive adsorption of alcohol/water monomers and dimers on the other site. The postulate of surface alkoxides being involved in ether synthesis does not contradict the mechanism for olefin synthesis because the sites involved in unimolecular and bimolecular alcohol dehydration on γ-Al_2O_3 are distinct.[19,31] The two-site model and the trimer inhibition model that involves a single site are kinetically indistinguishable, and experimentally, we cannot establish the involvement of alkoxide and physisorbed species under reaction conditions. Therefore, we discuss both models with the understanding that each of these models results in the correct asymptotic behavior of ether synthesis rates at high alcohol pressures which cannot be correctly explained by a model that considers only monomers and dimers adsorbed on to a single type of catalytic center.

Previously, we reported a model for diethyl ether (DEE) synthesis from EtOH that did not consider the involvement of alcohol dimer/water monomer trimers.[19] We have re-assessed these data with the trimer model for ether formation proposed above (eq 4) and note from the results shown in Figure 4 and

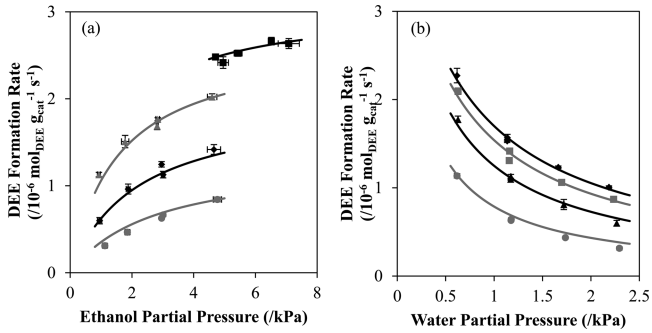

Figure 4. DEE formation rate for EtOH dehydration at 488 K on γ-Al_2O_3 (a) as a function of EtOH partial pressure with (black square) 0.41, (gray triangle) 0.62, (black diamond) 1.2, and (gray circle) 2.3 kPa water co-feeds and (b) as a function of water partial pressure with (black diamond) 7.1, (gray square) 4.8, (black triangle) 2.7, and (gray circle) 1.1 kPa EtOH co-feeds (total gas flow rate = 3.4 cm^3 s^{-1}). The solid line represents the model fits to eq 4

Table 11. Estimated Kinetic Parameters of DEE Formation from EtOH on γ-Al_2O_3 at 488 K Using the Model Presented in Equation 4 and Data from Figure 4

parameter	k_{DEE} (10^{-6} mol_{DEE} g_{cat}^{-1} s^{-1})	$(K'_{AW})/(K_{A1}K_{A2})$	$(K'_T)/(K_{A1}K_{A2})$ (kPa^{-1})
estimated value	4.40	4.04	1.02

DOI: 10.1021/cs501471r
ACS Catal. 2015, 5, 602−612

the parameters presented in Table 11 that this model fits the experimental results within error and both qualitatively and quantitatively describes the data better than the dimer model that we had postulated previously.[19]

The existence of di- and trimeric surface species on solid acids at these low-temperature conditions has been noted spectroscopically as discussed and indirectly inferred from measured rate dependences for a variety of reaction systems involving polar molecules. These examples include inhibition of esterification and dehydration rates on medium and large pore zeolites[32,33] as well as formation of water clusters.[30,34] The existence of multimeric surface adsorbates, therefore, is a general phenomenon for polar molecules at low temperatures, and their catalytic role is to inhibit the activation and conversion of the monomer/dimer surface adsorbate by competitive adsorption. Specifically, a more complete kinetic rate expression for bimolecular dehydration reactions discussed above should include terms corresponding to water trimers, alcohol trimers, and alcohol monomer/water dimers; however, the conditions used in this research and the observed pressure dependences are such that they allow us to exclude these terms.

3.4. Pyridine Titration of Active Sites for Bimolecular Dehydration. Pyridine is reversibly adsorbed on Lewis acidic sites of γ-Al_2O_3 and inhibits both unimolecular and bimolecular alcohol dehydration rates.[19,31] The number of active sites for ether formation was inferred by considering each adsorbed pyridine molecule to titrate one site and linearly extrapolating the initial slope of measured ether synthesis rates (see Figure 2 in DeWilde et al.[19]). In situ pyridine titration for EtOH, 1-PrOH, 2-PrOH, and *i*BuOH bimolecular dehydration on γ-Al_2O_3 at different pyridine pressures (0.02 and 0.05 kPa) and different catalyst weights (0.05, 0.1, and 0.2 g) resulted in similar pyridine uptakes for the different alcohols, as shown in Table 12, implying that the active sites for ether formation are

Table 12. Average Number of Sites for Bimolecular Dehydration Assessed Using In Situ Pyridine Titration at 488 K[a]

	EtOH	1-PrOH	2-PrOH	*i*BuOH
number of adsorbed pyridine (10^{-5} mol g_{cat}^{-1})	6.3 ± 1.9	5.4 ± 0.7	7.2 ± 0.4	8.0 ± 0.2

[a]The 95% confidence intervals were determined based on independent titrations.

independent of alcohol carbon number and branching. The numbers reported in Table 12 are in line with density functional theory calculations from Digne et al.[35] that report ~0.4 nm^{-2} surface densities of hydroxyl-group-free Al surface Lewis acid sites at 450 K.

Previously, we have used in situ pyridine titration to show that the number of active sites for bimolecular dehydration exceeds those for unimolecular dehydration at 623 K.[36] The distinct site requirements for bimolecular and unimolecular dehydration can also be indirectly inferred from the observation that the rate expressions have different denominator terms, a nonphysical scenario if the active sites were common. Given the diversity of coordination and hydration of Al and O species on γ-Al_2O_3 surfaces, this is not surprising; however, this distinction is often overlooked in mechanistic and computational chemistry studies. The number of active centers available for catalysis is expected to be a strong function of the temperature and reaction environment, particularly the presence of water, and can be rigorously probed by in situ methods such as pyridine titration that we describe above.

3.5. Effects of Substitution and Carbon Chain Length on Olefin Selectivity. EtOH, 1-PrOH, 2-PrOH, and *i*BuOH show different olefin formation rates and selectivity. A comparison of the rate constants and selectivity of olefin formation is represented in Table 13 (The rate constant for EtOH unimolecular dehydration is from data in Supporting Information, Table S1 and Figure S2). EtOH has the lowest rate constant of olefin formation, 3.40×10^{-7} $mol_{C_2H_4}$ g_{cat}^{-1} s^{-1}; the constants for 1-PrOH and *i*BuOH are similar in magnitude, 1.20×10^{-6} $mol_{C_3H_6}$ g_{cat}^{-1} s^{-1} and 3.29×10^{-6} $mol_{C_4H_8}$ g_{cat}^{-1} s^{-1}, respectively, and 2-PrOH has the highest rate constant, 4.13×10^{-5} $mol_{C_3H_6}$ g_{cat}^{-1} s^{-1}. Olefin formation involves an E2-type mechanism wherein the C−O and C−H bonds on C_β are broken.[8,18,27] Knözinger and co-workers[18,27] postulated the transition state for unimoelcular dehydration to involve C−O bond elongation resulting in positive charge (δ+) on C_α to explain the *trans*-elimination of water and the *cis*-preference in olefinic products, as shown in Scheme 4. Roy et al.[8] proposed

Scheme 4. Suggested Transition State for Unimolecular Dehydration of Alcohol on γ-Al_2O_3[a]

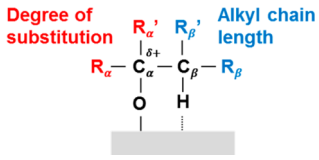

[a]From refs 8, 18, and 27. C_α has positive charge and H on C_β interacts with the catalyst surface. R_α, R_α', R_β, and R_β' can be a hydrogen or alkyl group.

the same transition state for unimolecular EtOH dehydration using cluster-based density functional theory calculations. Additional alkyl groups on C_α enhance stability of the carbocationic transition state because of electron donation. Kosteskyy et al.[37] compared dehydration barriers of C_2−C_4 alcohols on Al_2O_3, TiO_2, and ZrO_2 via a concerted E2 mechanism using cluster-based DFT calculations in Gaussian

Table 13. Rate constants of olefin and ether formation and selectivity to the olefin product for different alcohols on γ-Al_2O_3 with 2.4 kPa of alcohol and 1.0 kPa of water partial pressure at 488 K

	EtOH	1-PrOH	2-PrOH	*i*BuOH
rate constant of olefin formation (mol_{olefin} g_{cat}^{-1} s^{-1})	3.40×10^{-7}	1.20×10^{-6}	4.13×10^{-5}	3.29×10^{-6}
rate constant of ether formation (mol_{ether} g_{cat}^{-1} s^{-1})	4.40×10^{-6}	1.27×10^{-6}	3.08×10^{-6}	6.82×10^{-8}
selectivity to olefin[a] (%)	2.38	22.4	78.9	90.1

[a]Considering the stoichiometry, selectivity reported above is calculated as $(r_{olefin})/(r_{olefin} + 2r_{ether})$. The synthesis rates r_{olefin} and r_{ether} are calculated from the model equations for each alcohol species.

DOI: 10.1021/cs501471r
ACS Catal. 2015, 5, 602−612

(B3LYP/6-311G*) and noted that the barrier for dehydration decreased with increasing substitution of C_α. The maximum in temperature-programmed desorption profiles of C_2−C_4 alcohols dosed at submonolayer coverages on TiO_2 shifted to lower temperatures as substitution of the C_α increased,[38] consistent with an increase in rate constants for unimolecular dehydration that we assess. Olefin formation rate constants are of similar magnitude for alcohols with similar C_α substitution and increase dramatically (>10-fold) for 2-PrOH in reference to primary alcohols (see Table 13). The degree of substitution of C_β also affects the stability of the transition state because of inductive effects; however, because positive charge is predominantly on C_α and not on C_β, the effect of substituents on C_β is weaker than it is on C_α. The increased substitution on larger alcohols implies that 1-PrOH and *i*BuOH have higher olefin synthesis rate constants than EtOH (see Table 13). The preferential selectivity to more substituted olefins (Zaitsev products) in C_4−C_6 alcohol dehydration led Knözinger and coworkers[27] to infer that this was a consequence of increased substitution of C_β. Kim et al.[38] in the above referenced temperature-programmed desorption study on TiO_2(110) single crystals noted that the temperature corresponding to the maximum rate of desorption decreased as the degree of substitution of both C_α and C_β increased, with the degree of the substitution of C_α having the stronger effect on desorption temperature. The results of the study mirror the results of our kinetic analysis. The observed trends in rate constants for unimolecular dehydration of C_2−C_4 alcohols presented in Table 13 are consistently explained by the predominance of substitution effects on C_α and weaker dependence of rate parameters on C_β substitution as also noted broadly by Venuto and Landis.[39]

Olefin selectivity follows the same trend as the rate constant of unimolecular dehydration, except *i*BuOH. We surmise that this is a consequence of steric hindrance for bimolecular dehydration of *i*BuOH because of the steric bulk of alkyl groups which results in low selectivity to DiBE and correspondingly to a high olefin selectivity, as indicated by the lower rate constant for the bimoelcular dehydration of *i*BuOH. Clayborne et al.[40] also attributed the observed decrease in ether production in temperature-programmed desorption of C_1−C_5 alcohols on γ-Al_2O_3 to steric hindrance.

4. CONCLUSION

Primary kinetic isotope effects were observed for propene and isobutene formation on γ-Al_2O_3 when feeding deuterated 1-PrOH, 2-PrOH, or *i*BuOH reactants, implying that C−H bond cleavage (such as the C_β−H bond) is involved in the rate-determining step for olefin formation, which concurs with a similar observation for EtOH dehydration. The lack of a kinetic isotope for ether formation via bimolecular dehydration implies that C_α−O or Al−O bond cleavage is involved in the rate-determining step. Water inhibition was observed for both olefin and ether formation on γ-Al_2O_3. Steady-state kinetic studies show that olefin synthesis rates for unimolecular C_3−C_4 alcohol dehydration are inhibited by the alcohol reactant at high partial pressures and low partial pressure of water, in agreement with previous observations for ethene formation from EtOH. The unimolecular dehydration mechanism previously reported for EtOH is, therefore, confirmed as valid for C_2−C_4 alcohols on γ-Al_2O_3 at low-temperature conditions. The positive dependence of ether formation rates on alcohol pressure at low values and the asymptotic convergence to different rates depending on water pressure at high alcohol partial pressures implicates the involvement of either trimeric species or two sites. These kinetically indistinguishable models rigorously predict ether formation rates via bimolecular C_2−C_4 alcohol dehydration. 2-PrOH has the highest olefin formation constant, while EtOH has the lowest, indicating that C_α carbocation stability is the most important factor in determining olefin formation rates. In situ pyridine inhibition experiments show that the number of active sites for ether formation is the same irrespective of the carbon chain length and branching of the alcohol; this number is likely a function of reaction temperature. The quantitative assessment of rate and equilibrium parameters in this study enables the systematic assessment of carbon chain length and substitution as drivers for olefin selectivity in alcohol dehydration reactions that are useful from an industrial perspective and as probe reactions for assessing the reactivity of metal oxide surfaces.

■ ASSOCIATED CONTENT

Supporting Information

The following file is available free of charge on the ACS Publications website at DOI: 10.1021/cs501471r.

Kinetic dependences of C_3−C_4 alcohol unimolecular dehydration rates at low alcohol pressure and high water pressure, kinetic dependence of ethanol unimolecular dehydration rate, and analysis of residual error in the kinetic models for C_3−C_4 alcohol dehydration (PDF)

■ AUTHOR INFORMATION

Corresponding Author

*E-mail: abhan@umn.edu. Tel.: 612-626-3981. Fax: 612-626-7246.

Notes

The authors declare no competing financial interest.

■ ACKNOWLEDGMENTS

We appreciate financial support from The Dow Chemical Company. We also acknowledge Dr. Jeremy W. Bedard for helpful technical discussions.

■ REFERENCES

(1) Chorkendorff, I.; Niemantsverdriet, J. W. *Catalyst Supports: Alumina*; Wiley-VCH: Weinheim, Germany, 2007; Vol. 2, pp 193−195.
(2) *Industrial Minerals & Rocks*, 7th ed.; Kogel, J. E., Trivedi, N. C., Barker, J. M., Krukowsk, S. T., Eds.; Society for Mining, Metallurgy, and Exploration: Englewood, CO, 2006; 1568 pp.
(3) Lippens, B. C.; de Boer, J. H. *Acta Crystallogr.* **1964**, *17*, 1312−1321.
(4) Golay, S.; Doepper, R.; Renken, A. *Chem. Eng. Sci.* **1999**, *54*, 4469−4474.
(5) Knözinger, H. *Angew. Chem., Int. Ed.* **1968**, *7*, 791−805.
(6) Parry, E. *J. Catal.* **1963**, *2*, 371−379.
(7) Ripmeester, J. *J. Am. Chem. Soc.* **1983**, *105*, 2925−2927.
(8) Roy, S.; Mpourmpakis, G.; Hong, D.; Vlachos, D.; Bhan, A.; Gorte, R. *ACS Catal.* **2012**, *2*, 1846−1853.
(9) Christiansen, M. A.; Mpourmpakis, G.; Vlachos, D. G. *ACS Catal.* **2013**, *3*, 1965−1975.
(10) Knözinger, H.; Ratnasamy, P. *Catal. Rev. Sci. Eng.* **1978**, *17*, 31−70.
(11) Digne, M.; Sautet, P.; Raybaud, P.; Euzen, P.; Toulhoat, H. *J. Catal.* **2004**, *226*, 54−68.
(12) Dabbagh, H. A.; Zamani, M.; Davis, B. H. *J. Mol. Catal. A Chem.* **2010**, *333*, 54−68.

DOI: 10.1021/cs501471r
ACS Catal. 2015, 5, 602−612

(13) Wischert, R.; Laurent, P.; Copéret, C.; Delbecq, F.; Sautet, P. *J. Am. Chem. Soc.* **2012**, *134*, 14430−14449.
(14) Kwak, J. H.; Mei, D.; Peden, C. H. F.; Rousseau, R.; Szanyi, J. *Catal. Lett.* **2011**, *141*, 649−655.
(15) Golay, S.; Doepper, R.; Renken, A. *Appl. Catal. A Gen.* **1998**, *172*, 97−106.
(16) Cai, S.; Sohlberg, K. *J. Mol. Catal. A Chem.* **2003**, *193*, 157−164.
(17) Kwak, J. H.; Rousseau, R.; Mei, D.; Peden, C. H. F.; Szanyi, J. *ChemCatChem.* **2011**, *3*, 1557−1561.
(18) Knözinger, H.; Scheglila, A. *J. Catal.* **1970**, *17*, 252−263.
(19) DeWilde, J. F.; Chiang, H.; Hickman, D. A.; Ho, C. R.; Bhan, A. *ACS Catal.* **2013**, *3*, 798−807.
(20) Shi, B.; Davis, B. *J. Catal.* **1995**, *157*, 359−367.
(21) Knözinger, H.; Bühl, H.; Ress, E. *J. Catal.* **1968**, *12*, 121−128.
(22) Shi, B.; Dabbagh, H.; Davis, B. *Top. Catal.* **2002**, *18*, 259−264.
(23) Pines, H.; Haag, W. *J. Am. Chem. Soc.* **1961**, *83*, 2847−2852.
(24) Macht, J.; Janik, M. J.; Neurock, M.; Iglesia, E. *Angew. Chem., Int. Ed.* **2007**, *46*, 7864−78688.
(25) Greenler, R. G. *J. Chem. Phys.* **1962**, *37*, 2094−2100.
(26) Gabrienko, A.; Arzumanov, S.; Toktarev, A.; Stepanov, A. *J. Phys. Chem. C* **2012**, *116*, 21430−21438.
(27) Knözinger, H.; Bühl, H.; Kochloefl, K. *J. Catal.* **1972**, *24*, 57−68.
(28) Rep, M.; Palomares, A. E.; Eder-Mirth, G.; van Ommen, J. G.; Rösch, N.; Lercher, J. A. *J. Phys. Chem. B* **2000**, *104*, 8624−8630.
(29) Schenkel, R.; Jentys, A.; Parker, S. F.; Lercher, J. A. *J. Phys. Chem. B* **2004**, *108*, 15013−15026.
(30) Wang, C.; Bai, P.; Siepmann, J. I.; Clark, A. E. *J. Phys. Chem. C* **2014**, *118*, 19723−19732.
(31) Jain, J.; Pillai, C. *J. Catal.* **1967**, *9*, 322−330.
(32) Bedard, J.; Chiang, H.; Bhan, A. *J. Catal.* **2012**, *290*, 210−219.
(33) Chiang, H.; Bhan, A. *J. Catal.* **2010**, *271*, 251−261.
(34) Joshi, K. L.; Psofogiannakis, G.; van Duin, A. C. T.; Raman, S. *Phys. Chem. Chem. Phys.* **2014**, *16*, 18433−18441.
(35) Digne, M.; Sautet, P.; Raybaud, P.; Euzen, P.; Toulhoat, H. *J. Catal.* **2002**, *211*, 1−5.
(36) DeWilde, J. F.; Czopinski, C. J.; Bhan, A. *ACS Catal.* **2014**, *4*, 4425−4433.
(37) Kostestkyy, P.; Yu, J.; Gorte, R. J.; Mpourmpakis, G. *Catal. Sci. Technol.* **2014**, *4*, 3861−3869.
(38) Kim, Y. K.; Kay, B. D.; White, J. M.; Dohnálek, Z. *Catal. Lett.* **2007**, *119*, 1−4.
(39) Venuto, P. B.; Landis, P. S. *Adv. Catal.* **1968**, *18*, 259−371.
(40) Clayborne, P.; Nelson, T.; DeVore, T. *Appl. Catal., A* **2004**, *257*, 225−233.

DOI: 10.1021/cs501471r
ACS Catal. 2015, 5, 602−612